AD-775 614

UNIFIED RANGE SPECTRUM AND LET DISTRI-
BUTION FOR HZE PARTICLES OF GALACTIC
RADIATION IN SPACE

Hermann J. Schaefer

Naval Aerospace Medical Research Laboratory

AD-775614

DOCUMENT CONTROL DATA - R & D

Security classification of title, body of abstract and indexing annotation must be entered when the overall report is classified)

1. ORIGINATING ACTIVITY (Corporate author)	2a. REPORT SECURITY CLASSIFICATION
Naval Aerospace Medical Research Laboratory Pensacola, Florida	Unclassified
	2b. GROUP

3. REPORT TITLE

Unified Range Spectrum and LET Distribution for HZE Particles of Galactic Radiation in Space

4. DESCRIPTIVE NOTES (Type of report and inclusive dates)

N/A

5. AUTHOR(S) (First name, middle initial, last name)

Hermann J. Schaefer

6. REPORT DATE	7a. TOTAL NO. OF PAGES	7b. NO. OF REFS
14 December 1973	26	4
8a. CONTRACT OR GRANT NO. NASA W-13,280	9a. ORIGINATOR'S REPORT NUMBER(S)
b. PROJECT NO.	NAMRL-1198
c.	9b. OTHER REPORT NO(S) (Any other numbers that may be assigned this report)
d.	48

10. DISTRIBUTION STATEMENT

Approved for public release; distribution unlimited.

11. SUPPLEMENTARY NOTES	12. SPONSORING MILITARY ACTIVITY
Prepared for the National Aeronautics and Space Administration	

13. ABSTRACT

A unified range spectrum for the flux densities of HZE particles of galactic radiation in space is presented for establishing the individual spectrum for any Z number with a simple scaling procedure. Data on Z abundances are presented and the Z spectrum from $Z = 2$ to 28 is divided into four classes. Range spectra for the class representatives are derived. The influence of the geomagnetic cutoff on the range spectra for different latitudes is discussed. The data are summarized in two graphs from which event sizes in terms of LET and related track lengths and their frequencies for given target volumes can be read directly.

DD FORM 1473 (PAGE 1)

S/N 0101-807-6801

14 KEY WORDS	LINK A		LINK B		LINK C	
	ROLE	WT	ROLE	WT	ROLE	WT
Space radiation dosimetry						
HZE particles in space, unified range spectrum for						
HZE particles in space, LET distribution of						

UNIFIED RANGE SPECTRUM AND LET DISTRIBUTION FOR HZE PARTICLES

OF GALACTIC RADIATION IN SPACE

Hermann J. Schaefer

NASA Order No. W-13,280
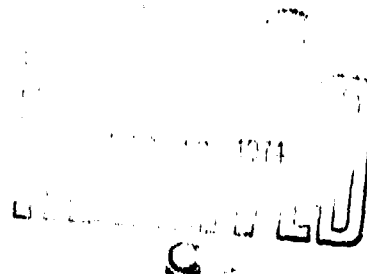
Approved by
Ashton Graybiel, M.D.
Assistant for Scientific Programs

Released by
Captain N. W. Allebach, MC USN
Officer in Charge

14 December 1973

SUMMARY PAGE

   In a preceding report, the basic physics of attenuation and energy dissipation of galactic heavy primaries (so-called HZE particles) in matter was reviewed. However, application to actual spectra of the various Z components of galactic radiation in space was limited to alpha particles ($Z = 2$) and the iron group ($Z = 26$).

   The present report supplements the earlier one by furnishing complete information on all Z components of the primary radiation. A graph and tabulation of the unified range spectrum for solar minimum and maximum is presented and the arithmetic operation explained for deriving, from the unified spectrum, the range spectrum for any Z component. The Z spectrum is divided into four groups and a specific Z number selected as representative for each group. The range spectra of the incident radiation for the four representatives are derived and the depth distributions of enders established. The screening effect of the geomagnetic field is examined and cutoff ranges at different latitudes derived.

   In a final section, the results are evaluated microdosimetrically. The LET and related track length distributions in tissue are established and summarized in two graphs intended to assist the radiobiological experimenter in extracting direct information on event frequencies and sizes for given target volumes.

INTRODUCTION

In an earlier report (1), hereafter referred to as Report 1172, the basic physics of energy dissipation of HZE particles in matter and the relationships between energy, range and linear energy transfer (LET) in tissue is reviewed. The same report also summarizes the state of knowledge of galactic HZE particle flux densities at solar minimum and maximum. The latter data, however, are presented only for the alpha component as reference and the Fe group ($Z = 26-28$). The present report supplements Report 1172 and furnishes complete information on the entire heavy spectrum. Data are presented, wherever feasible, with range as independent variable because range has the distinct advantage over energy that it applies very directly to questions concerning shielding effects or depth dose distributions.

As pointed out in Report 1172, experimental findings indicate that all components of the primary galactic radiation with Atomic Number $Z = 2$ and higher show identical configurations of the energy spectrum if flux density is plotted as function of energy per nucleon. While this allows a unified presentation for all Z components, such presentation lacks the just mentioned advantage of a plot of flux density as function of range because particles of different Z have, for the same energy per nucleon, different ranges. However, these ranges are related by the constant scaling factor A/Z^2 where A is the Mass Number. Similarly, differential flux density per unit energy interval is related to the same quantity per unit range interval by the constant scaling factor Z^2/A. Therefore, if the indicated multiplication of flux density and division of range by Z^2/A is accepted, a unified presentation of the range spectrum for all Z species can be accomplished.

THE UNIFIED RANGE SPECTRUM

Figure 1 shows the unified range spectrum for solar minimum and maximum. The spectra are identical with those shown in Figure 6 on page 22 of Report 1172. The earlier plot is merely extended downward to 0.1 g/cm^2. It should be pointed out, though, that this extension is partly based on extrapolation since experimental data are scarce below 1 g/cm^2. This limitation is due to the fact that vehicle frame and wall of the sensing device impose, on any instrument design, an inherent shielding, the so-called instrument cutoff, below which data on flux densities simply cannot be acquired.

For different Z numbers a given instrument cutoff range corresponds to different cutoff energies. Consulting the range/energy function for selected Z numbers in Figure 2 we see that an instrument cutoff of, e.g., 0.2 g/cm^2 corresponds to quite different energies ranging from 22.5 Mev/nucleon for C - nuclei ($Z = 6$) to 49 Mev/nucleon for Fe nuclei ($Z = 26$). Locating these cutoff points in the energy spectra of Figure 5 in Report 1172 one obtains a more realistic picture to what extent the proposition of identical configuration of the energy spectrum for all Z numbers is actually proven by measurements. The basic reference spectra in Figure 1 are derived from

1

measurements reported by Meyer (2) and Mason (3) for the alpha component (Z = 2) with a lowest energy of 12 Mev/nucleon corresponding to an instrument cutoff of about 0.2 g/cm^2. That instrument cutoff corresponds, for higher Z numbers, to cutoff energies substantially greater than 12 Mev/nucleon. It is seen, then, that for higher Z numbers, the proposition of identical spectral configuration is not adequately established for the left-hand sections of the spectra in Figure 5 of Report 1172.

The lack of direct experimental data for low-range particles of high Z is well demonstrated in the just quoted paper by Meyer (2). It is seen there that, for instance, recordings of Silicon nuclei (Z = 14) have been reported only down to an energy of 80 Mev/nucleon corresponding to an instrument cutoff of 1.3 g/cm^2. Since assessments of HZE particle effects on man always center on high Z numbers such as Fe nuclei (Z = 26) or the Z $\geq$ 20 group, the pitfalls of indiscriminate use of the unified spectrum for estimating hit frequencies should be obvious. At the present state of knowledge, such estimates carry a large margin of uncertainty and could never replace actual recordings with suitable detectors on the body of the astronaut. These limitations should also be kept in mind when we proceed now to establish the range spectra for various Z groups from the unified spectra in Figure 1.

Since alpha particles (He, Z = 2, A = 4) have the unique property that the factor Z^2/A equals 1.0, multiplication of flux density or division of range by the factor does not change these quantities. Furthermore, the ordinate scale in Figure 1 is normalized to the flux density of alpha particles. In other words, the abundance factor for alpha particles in Figure 1 is equal to 1.0. With all factors equal to unity, the spectra directly represent the alpha component. For conversion to higher Z numbers the ordinate values read from the curves have to be multiplied by Z^2/A and the abundance factor F and the abscissa values divided by Z^2/A. With these operations any pair of values for flux density and range read from Figure 1 can be converted to a corresponding pair for any Z species. In this conversion, the operations with the factor Z^2/A reflect a basic relationship of nuclear physics and therefore carry no experimental error. The abundance factor F, however, is strictly an empirical quantity reflecting the make-up of the galactic spectrum as determined by measurements.

ABUNDANCES OF DIFFERENT Z NUMBERS

For any nuclear-particle detector, Z discrimination involves a complex technique which unavoidably carries an error margin of plus minus one to several units of Z. Accuracy is further impaired by poor statistics since higher Z numbers have a much smaller flux density than the alpha component. These limitations have led to the common practice of expressing recordings in terms of flux densities for Z-groups rather than individual Z numbers. Nevertheless, estimates of relative abundances of specific elements, at least for medium heavy nuclei, have been reported. Without attempting a complete and critical review, we show in Table I data compiled by Meyer (2) with abundance factors normalized to unity for the Fe group (Z = 26). Abundances are expressed in terms of relative particle flux densities. The shares of heavier particles in the total energy fluence or the total ionization are much higher since for the former the

2

particle number has to be multiplied by the Mass Number A and for the latter by the square of the Atomic Number Z.

It should be mentioned in passing that HZE particles with Z numbers beyond 28 have been identified in the primary radiation (4). In fact, it appears that nuclei of all elements of the Periodic System are represented in the galactic radiation. However, these superheavy particles are extremely rare. Lumping them all together, one obtains an estimated particle flux density of 10^{-4} compared to the iron group as unity. Because of this extremely low frequency, it would appear far fetched to include superheavy nuclei in the present dosimetric analysis.

It was mentioned before that for an overall view of the basic characteristics it is greatly preferable to deal with Z groups rather than individual elements. For each group a representative element is selected in order to express energy, range and LET in specific terms whereas particle flux density is expressed for the total group. The system which we have selected for evaluating range spectra of higher Z species from the unified spectrum is shown in Table II. Contrary to Table I abundance factors in Table II are normalized to the flux density of alpha particles (He, Z = 2, A = 4) since the ordinate scale in Figure 1 as mentioned before directly denotes flux density.

Figures 3 through 6 show the differential range spectra for the four groups established by the indicated conversion of data from the unified spectra in Figure 1. The reader who would want to obtain more accurate values of ranges and related flux densities for the unified spectra is referred to Table III which presents the spectra of Figure 1 as tabulation in small incremental steps of range.

It is essential to have a clear understanding of the difference between the curves marked "Incident" and those marked "Reaching Depth R" in Figures 3-6. The former show the make-up of the radiation before it enters absorbing material. The latter, however, do not describe the make-up at any one location but denote the number of so-called enders, i.e., of particles coming to rest at various depths R. Since a particle shortly before it comes to rest passes through maximum LET in the Bragg peak, the curves marked "Reaching Depth R" directly show the distribution of the events of highest local energy dissipation in shield or tissue. For these curves, the term "per g/cm^2" in the ordinate notation assumes a different meaning. Enders per g/cm^2 means enders in a layer of unit thickness at depth R in the absorbing material. We read, for instance, from Figure 6 that at solar maximum slightly more than 10 Fe nuclei/(m^2 hours ster g/cm^2) reach depth 10 g/cm^2 in tissue. As just explained, this means that in a tissue slab of 1 m^2 cross section and 1 g/cm^2 (i.e., for density 1, 1 cm) thickness located at a depth of 10 g/cm^2 10 iron nuclei will terminate per hour incident from unit solid angle of the sky. Since the slab has a total volume of 10,000 cm^3, the ender density will be slightly more than $10 \times 10^{-4} = 0.001$ per cm^3 per hour per unit solid angle at a depth of 10 cm in tissue.

3

GEOMAGNETIC CUTOFF RANGES AND LATITUDES

In estimating HZE particle fluences for specific missions in near-Earth orbits, a very important parameter is the so-called geomagnetic cutoff. It reduces the fluence in an orbit of low inclination substantially as compared to an orbit of high inclination or a polar orbit. Simplifying the complex relationships governing the trajectories of charged particles in a magnetic dipole field, one can establish a satisfactory first approximation for the residual fluence at a given geomagnetic latitude by using the vertical cutoff, i.e., the minimum momentum of arrival from the vertical. Since the critical momentum depends on the fourth power of the cosine of geomagnetic latitude, the flux density of galactic particles reaching a vehicle in a near-Earth orbit is an extremely strong function of latitude. Converting particle momentum to energy per nucleon or to range, one can easily locate the cutoff points for given latitudes in the energy or range spectrum. In the present context, the dependence of the cutoff range on latitude is of special interest. Whereas the cutoff momentum or cutoff energy at a given latitude is the same for all particles with the same Z/A ratio, i.e., for all HZE particles, cutoff ranges for a given latitude are different for different Z species. Figure 7 shows the dependence of the cutoff range on latitude for selected Z numbers. The steep changes of the cutoff range with latitude are evident, for instance, if one compares critical ranges for a standard Gemini-type orbit with 30° inclination to those for the Skylab orbit with 50° inclination. In Figures 3 through 6, cutoff ranges for latitudes 30, 40, 50 and 60° are indicated with arrows on the abscissa scale. Again, the substantial decrease of particle fluence with decreasing latitude, especially for higher Z species, is striking. It is also seen that geomagnetic screening affects the enders frequency much more than the fluence of particles of medium and high penetrating powers. It is interesting to note in this connection that nuclear emulsions flown on all Gemini missions as well as the orbital missions Apollo 7 and 9 are completely void of enders of HZE particles of the $Z \geq 20$ class whereas such enders do occur in emulsions of the Skylab missions.

THE LET SPECTRUM

The reason for the distinction of enders from the remainder of the HZE particle fluence rests in their high LET. In the final analysis, the distinction is artificial inasmuch as the LET spectrum, in the same way as the energy and range spectrum, is a continuum containing all values from the minimum LET of a particle at relativistic speed to the maximum LET in the Bragg peak at very low speed. Since the LET spectrum is the important feature of an HZE particle radiation field from a radiobiological viewpoint, the range spectra in Figures 3-6 have to be converted to LET spectra. The Bragg curve, discussed in detail in Report 1172, directly relates instantaneous LET of a particle to its residual range. At first sight, the indicated conversion thus might appear a simple task. However, a certain difficulty arises from the fact that the incident range spectra are defined only down to 0.1 g/cm². That means the flux density of the radiobiologically most important section containing the high LET in the Bragg peak remains undetermined. The problem can be avoided by establishing the local LET spectrum behind a shielding layer of at least 0.1 g/cm². At depth 0.1 g/cm², particles with ranges less than

4

0.1 g/cm^2 are eliminated by absorption whereas those of exactly 0.1 g/cm^2 range terminate at the point of observation making the range spectrum at that point a continuum reaching down to zero range. Since the body of the astronaut will always be protected by layers of material substantially heavier than 0.1 g/cm^2, we have evaluated the local spectra behind a shielding layer of 1.0 g/cm^2.

In presenting a differential energy or range spectrum it is customary to quote flux density per unit energy or range interval throughout the entire energy or range scale. For LET spectra, a different approach is usually preferred and flux density is computed per unit interval of log LET rather than LET itself. Making numerical estimates for specific LET intervals from such plots requires an awkward log/antilog conversion. To facilitate such work, the LET spectra in Figures 8 to 10 are shown as histograms with flux densities shown for finite LET intervals of a constant width of 0.1 log units. The LET increments are also listed below the captions of Figures 8-10. Since the interest of the radiobiologist and health physicist centers on the fraction of the total particle fluence that carries LET values well above those of conventional radiations, the presentation of LET spectra in Figures 8-10 is limited to the upper end of the LET scale beginning at 100 kev/micron tissue. For the same reason, the Z spectrum is limited to particles of $Z \geq 10$. That means the C group ($Z = 3$ to 9) is omitted. In the histogram of the Fe group, a lower LET limit of 200 kev/μ T is used because the LET of Fe nuclei is always larger than 100 kev/μ T.

For HZE particles, the LET spectrum alone does not furnish a complete picture of the microdosimetric pattern of energy dissipation in tissue. Additional information is needed on the distribution of lengths over which individual track segments sustain certain LET levels. To be sure, the radiobiological significance of this distribution is at present not well understood. However, since a greater disuniformity of energy dissipation in the microstructure of tissue seems to cause greater tissue damage, the distribution in question is likely to constitute an important parameter for radiobiological experimentation with HZE particles. The uppermost histograms in Figures 8-10 to be read with the right-hand ordinates show the length distribution of track segments. Contrary to the flux density histograms, they represent integral distributions, i.e., they show segment lengths over which the LET is equal to or greater than the abscissa value.

At the upper end of the LET interval, resolution of both types of histograms in Figures 8-10 is rather poor. At the same time, these particular sections of the LET interval ending up in the Bragg peak are of particular importance radiobiologically since they contain the events of highest LET. Therefore, the sections are shown with a linear LET scale of higher resolution in Figure 11. The upper graph shows integral flux densities for the three Z groups at solar minimum. That means that, contrary to the corresponding histograms in Figures 8-10, the plot shows cumulative flux densities of particles with an LET equal to or greater than the abscissa value. For better descriptiveness, the dimensional unit of the ordinate scale of the upper graph of Figure 11 has been changed from "per m^2 per hour per unit solid angle" to "per cm^3 per day for 2 pi incidence". This way, estimates of hit frequencies for events at

5

various LET levels can be made with a minimum of arithmetic. Finally, the lower graph in Figure 11 shows the length distributions of track segments for the three Z groups over the same abscissa as the upper graph. No change of the type of distribution has been made in this plot as compared to the corresponding curves in Figures 8-10.

For the radiobiologist or health physicist trying to isolate, in the heterogeneous mixture of radiation fields in space, the specifically new type of radiation exposure due to HZE particles, the two graphs in Figure 11 summarize the essential information. They demonstrate concisely and quantitatively the basic features of HZE particle exposure: very high local concentration of energy dissipation in the individual event yet very low frequency of occurrence.

REFERENCES

1. Schaefer, H. J., Dosimetric characteristics of HZE particles in space. NAMRL-1172. Pensacola, Fla.: Naval Aerospace Medical Research Laboratory, 1972.

2. Meyer, P., Cosmic rays in the galaxy. Ann. Rev. of Astronomy and Astrophy. 7:1-38, 1969.

3. Mason, G. M., Interstellar propagation of galactic cosmic ray nuclei $2 \leq Z \leq 8$ in the energy range 10 - 1000 Mev per nucleon. J. Astrophy. 171:139-161, 1972.

4. Fowler, P. H., Adams, R. A., Cowen, V. G., and Kidd, J. M., The charge spectrum of very heavy cosmic ray nuclei. In: Proceedings of the Royal Society. London. 301:39-45, 1967.

Table I

Abundances of HZE Particles in the Primary Galactic Radiation
Normalized to Iron Group (Fe, Z = 26)

Element	Atomic Number, Z	Mass Number, A	Relative Abundance
He	2	4	300
Li	3	7	1.3
Be	4	9	0.6
B	5	11	2.2
C	6	12	6.7
N	7	14	1.6
O	8	16	6.7
F	9	19	0.03
Ne	10	20	1.2
Na	11	23	0.3
Mg	12	24	1.9
Al	13	27	0.2
Si	14	28	1.3
P-V	15-23	31-51	0.8
Cr-Ni	24-28	52-58	1.0

8

Table II

Z Groups and Group Representatives of the Heavy Components of Primary Galactic Radiation

Element	Atomic Number, Z	Group Representative,			Abundance Factor F	Minimum LET, kev/micron T	Z^2/A	$Z^2/A \times F$
		Element	Z	Mass Number, A				
He	2	-	-	-	1.00	0.80	1.00	1.00
Li – F	3–9	C	6	12	0.0633	7.2	3	0.19
Ne – Si	10–14	Mg	12	24	0.0167	29	6	0.10
P – Va	15–23	Ca	20	40	0.00257	80	10	0.0267
Cr – Ni	24–28	Fe	26	56	0.00333	135	12	0.040

9

Table III

The Unified Differential Range Spectrum for HZE Particles of Galactic Radiation

Range in Tissue, g/cm^2	Flux Density, Particles/(m^2 hr ster g/cm^2)		Range in Tissue, g/cm^2	Flux Density, Particles/(m^2 hr ster g/cm^2)	
	Solar Min	Solar Max		Solar Min	Solar Max
.10	11,700	1798	10	7310	1477
.125	11,180	1674	12.5	6960	1472
.15	10,680	1605	15	6640	1455
.175	10,260	1545	17.5	6340	1430
.20	10,050	1493	20	6060	1405
.25	9620	1405	25	5560	1349
.30	9340	1364	30	5140	1285
.35	9120	1336	35	4810	1224
.40	8950	1317	40	4520	1172
.50	8710	1287	50	4035	1080
.60	8600	1269	60	3600	1000
.70	8525	1260	70	3240	928
.80	8475	1254	80	2940	864
.90	8450	1251	90	2700	809
1.0	8440	1250	100	2480	759
1.25	8440	1254	125	2080	661
1.5	8460	1265	150	1780	585
1.75	8470	1277	175	1560	524
2.0	8460	1295	200	1380	473
2.5	8420	1325	250	1110	393
3.0	8360	1355	300	904	325
3.5	8280	1380	350	760	276
4.0	8190	1400	400	660	242
5.0	7980	1421	500	525	197
6.0	7865	1444	600	430	166
7.0	7745	1459	700	360	142
8.0	7605	1470	800	303	122
9.0	7455	1475	900	256	106
			1000	220	92.5
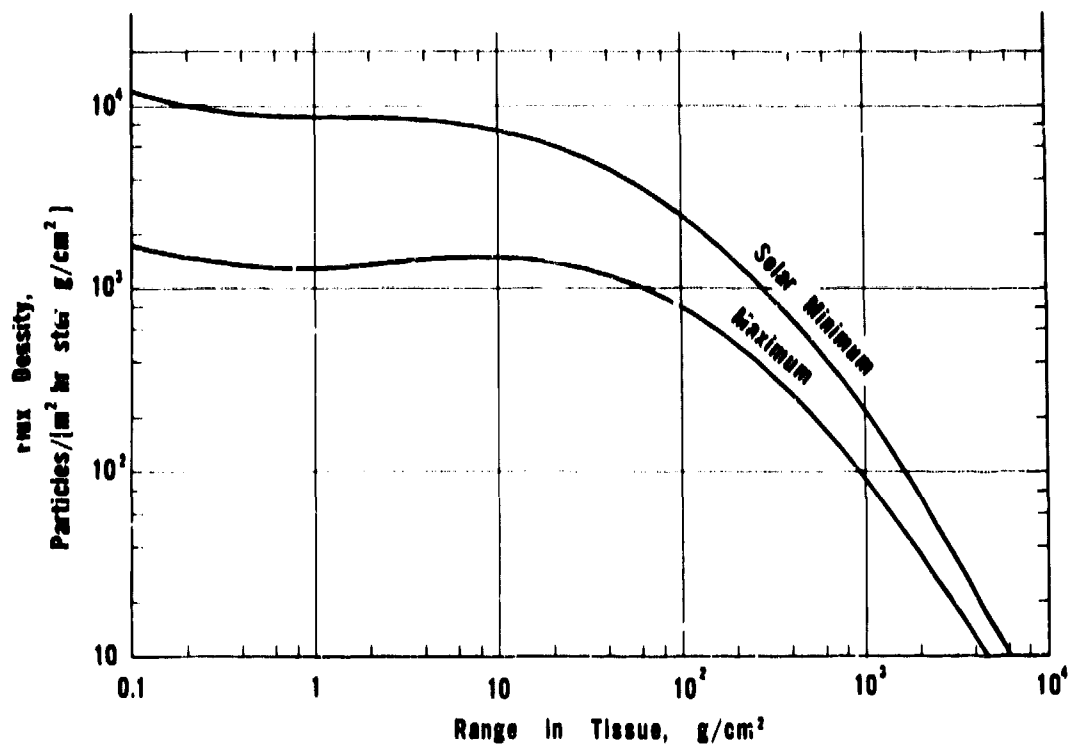
UNIFIED DIFFERENTIAL RANGE SPECTRA OF GALACTIC
HZE PARTICLES AT SOLAR MINIMUM AND MAXIMUM

FIGURE 1

Kinetic Energy, Mev/nucleon
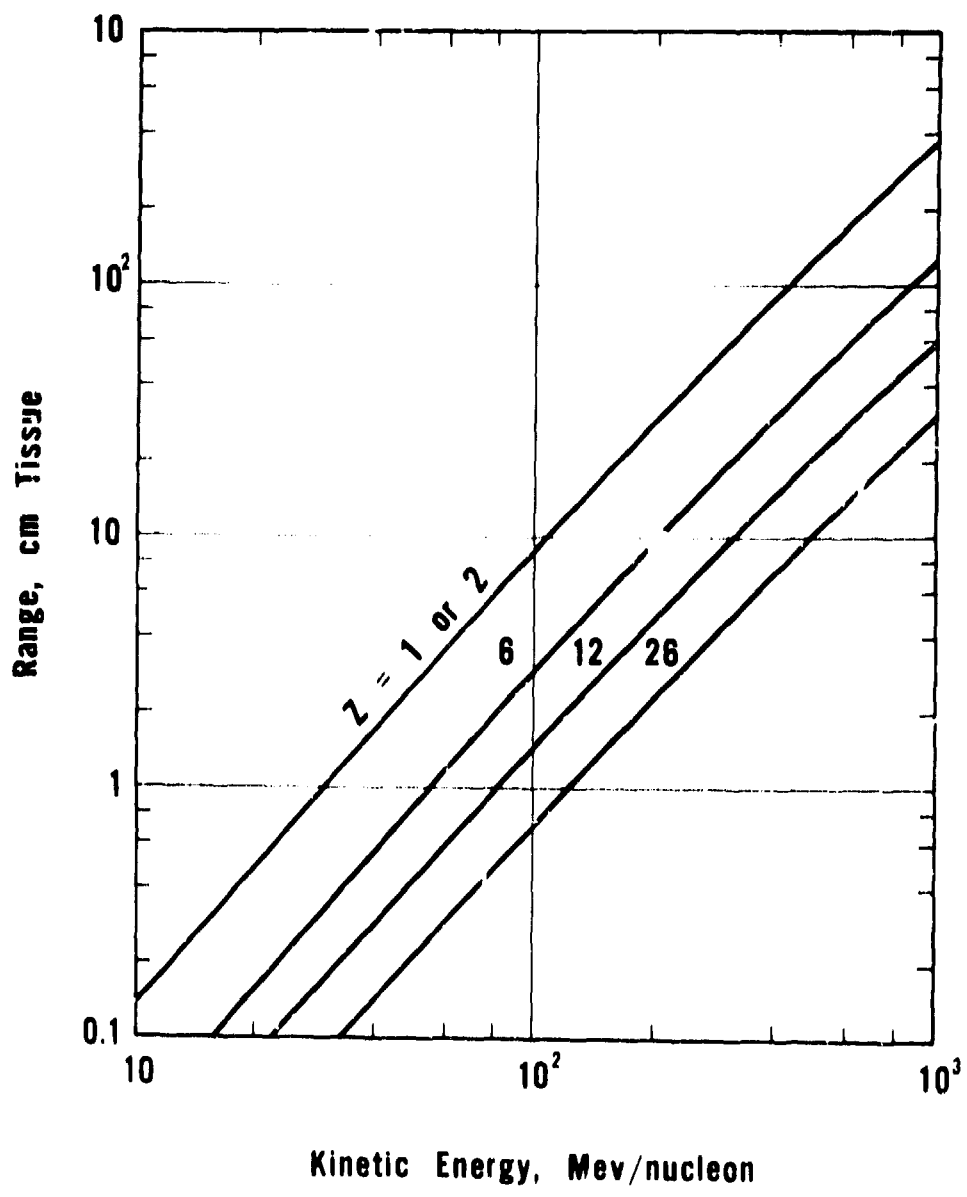
RANGE/ENERGY FUNCTION IN TISSUE
FOR NUCLEAR PARTICLES

FIGURE 2

12
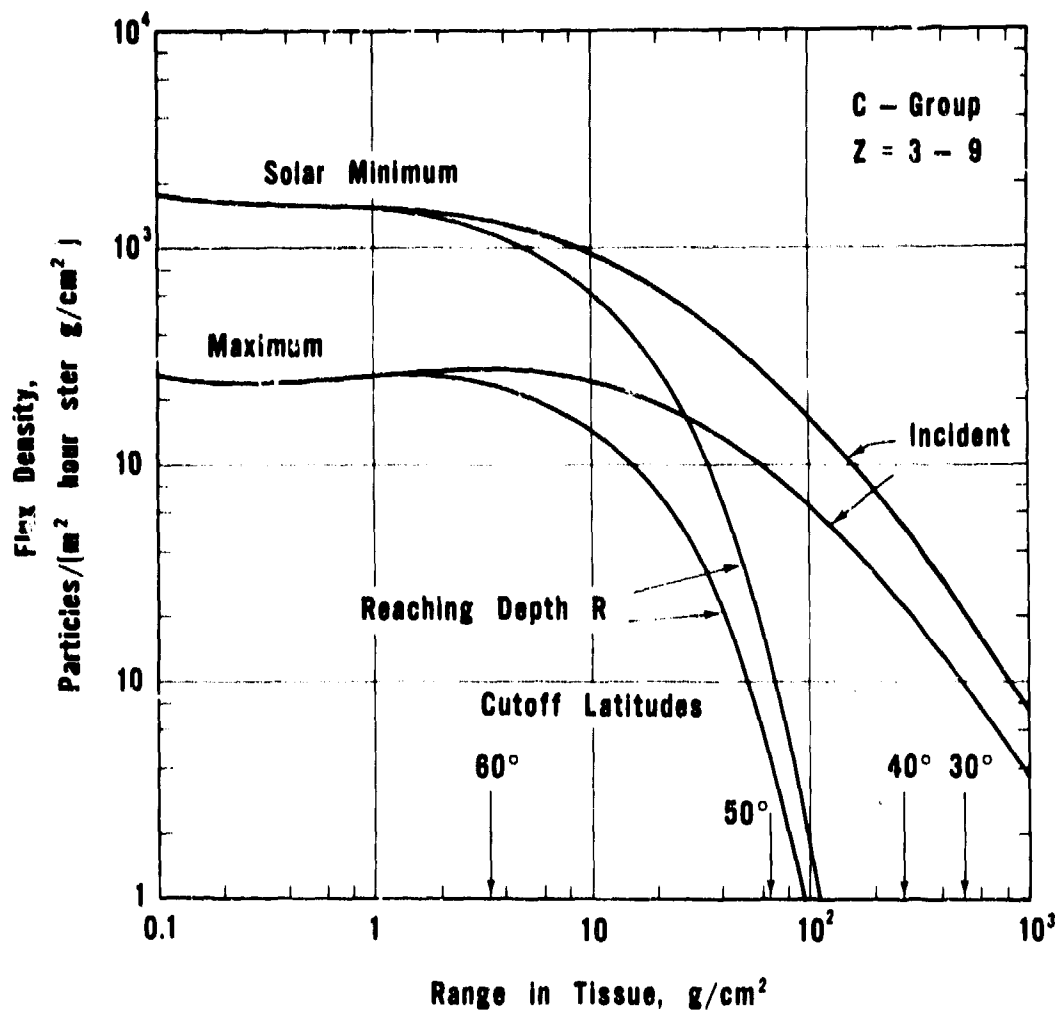
DIFFERENTIAL RANGE SPECTRA OF C — GROUP
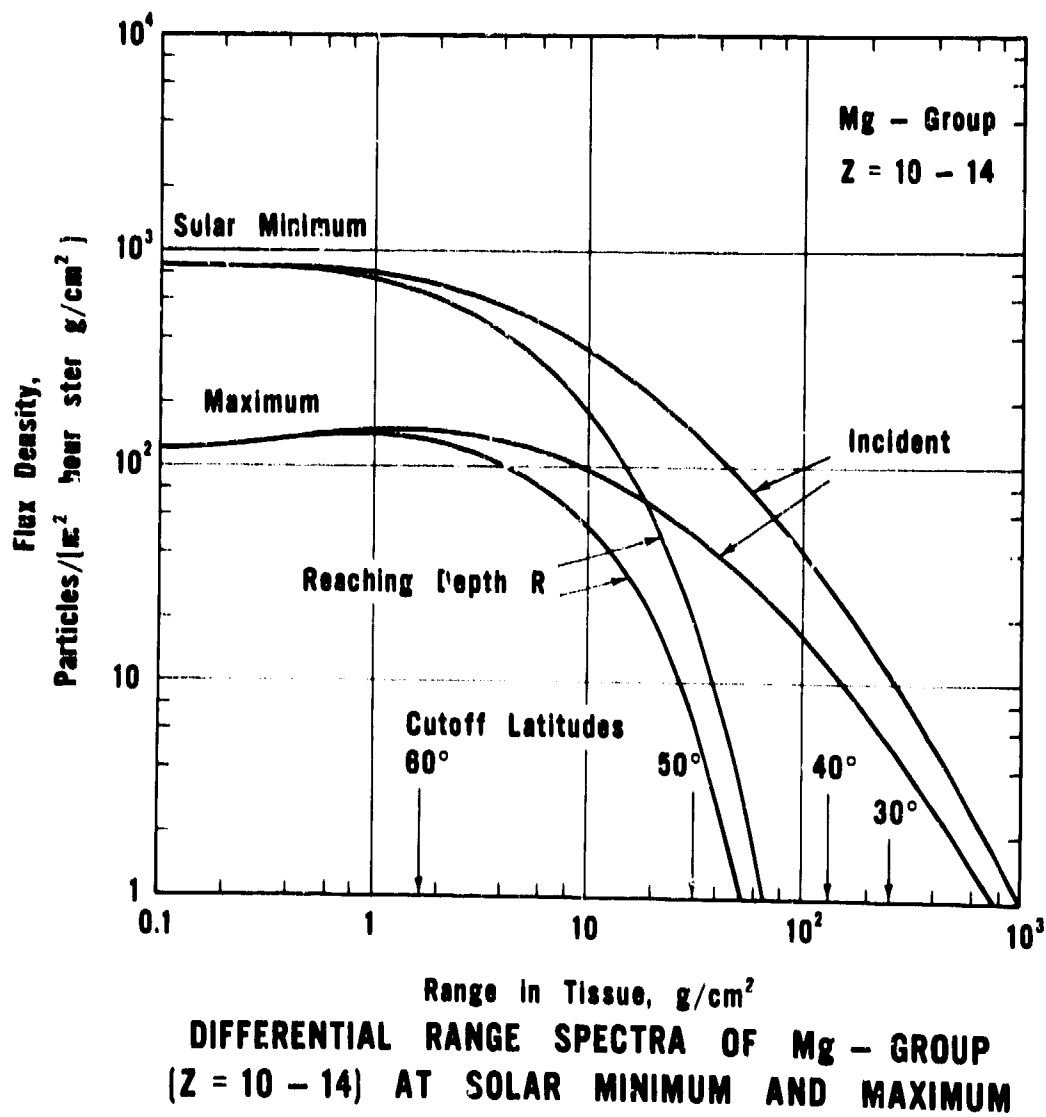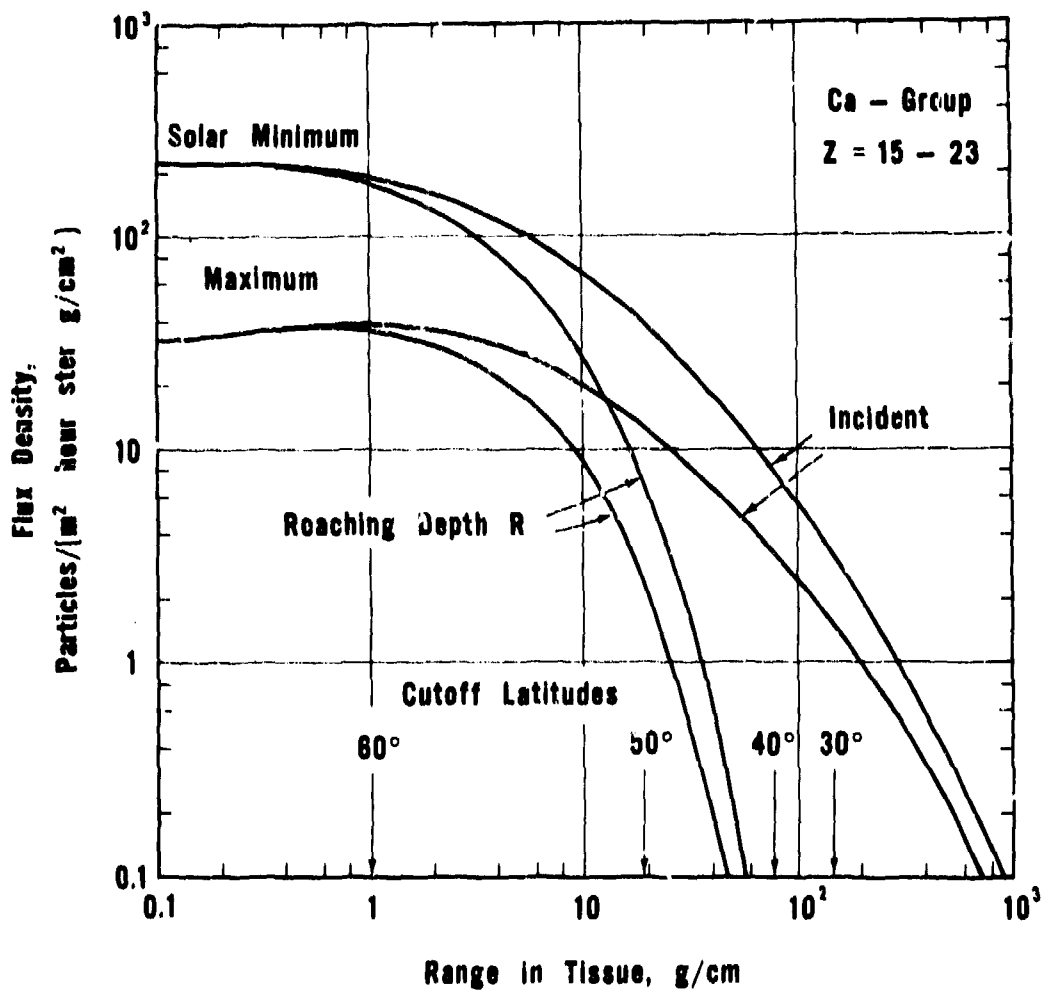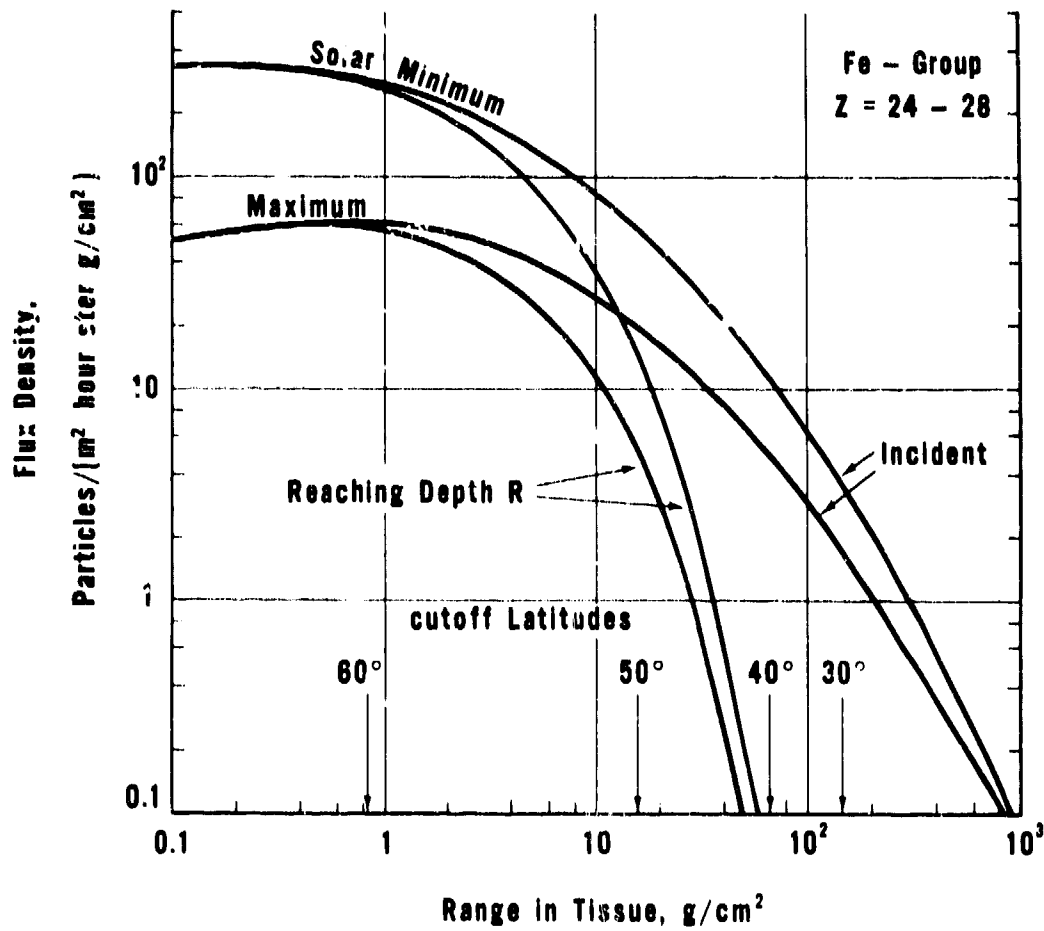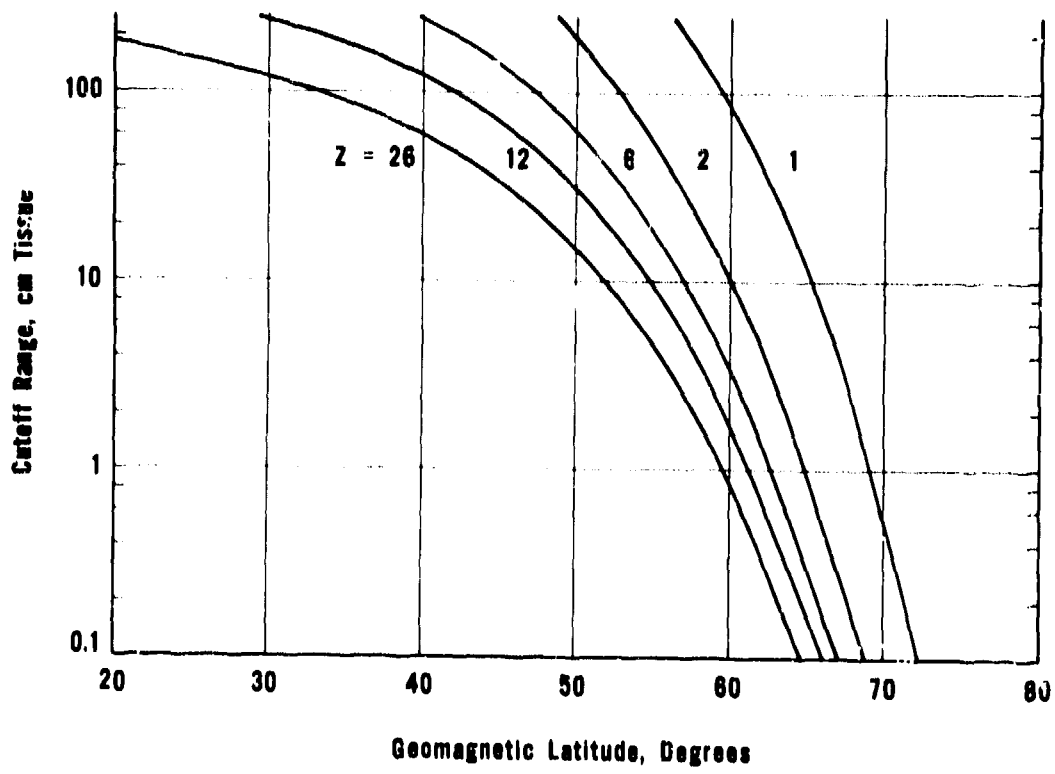(Z = 3 — 9) AT SOLAR MINIMUM AND MAXIMUM

FIGURE 3

DIFFERENTIAL RANGE SPECTRA OF Mg – GROUP (Z = 10 – 14) AT SOLAR MINIMUM AND MAXIMUM

FIGURE 4

14

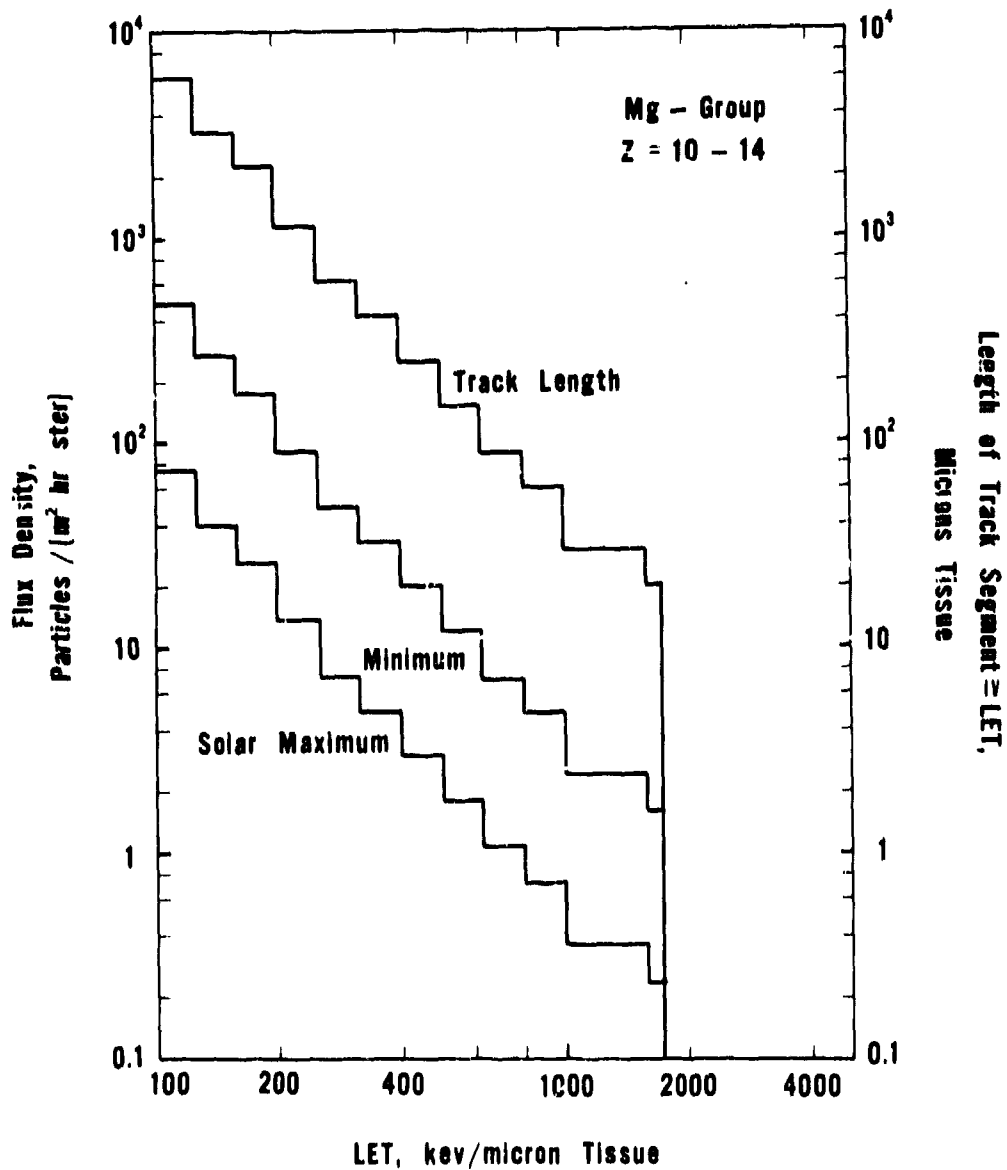**DIFFERENTIAL RANGE SPECTRA OF Ca – GROUP (Z = 15 – 23) AT SOLAR MINIMUM AND MAXIMUM**

FIGURE 5

DIFFERENTIAL RANGE SPECTRA OF Fe — GROUP
(Z=24–28) AT SOLAR MINIMUM AND MAXIMUM

FIGURE 6

16

LATITUDE CUTOFF RANGES FOR GALACTIC PARTICLES
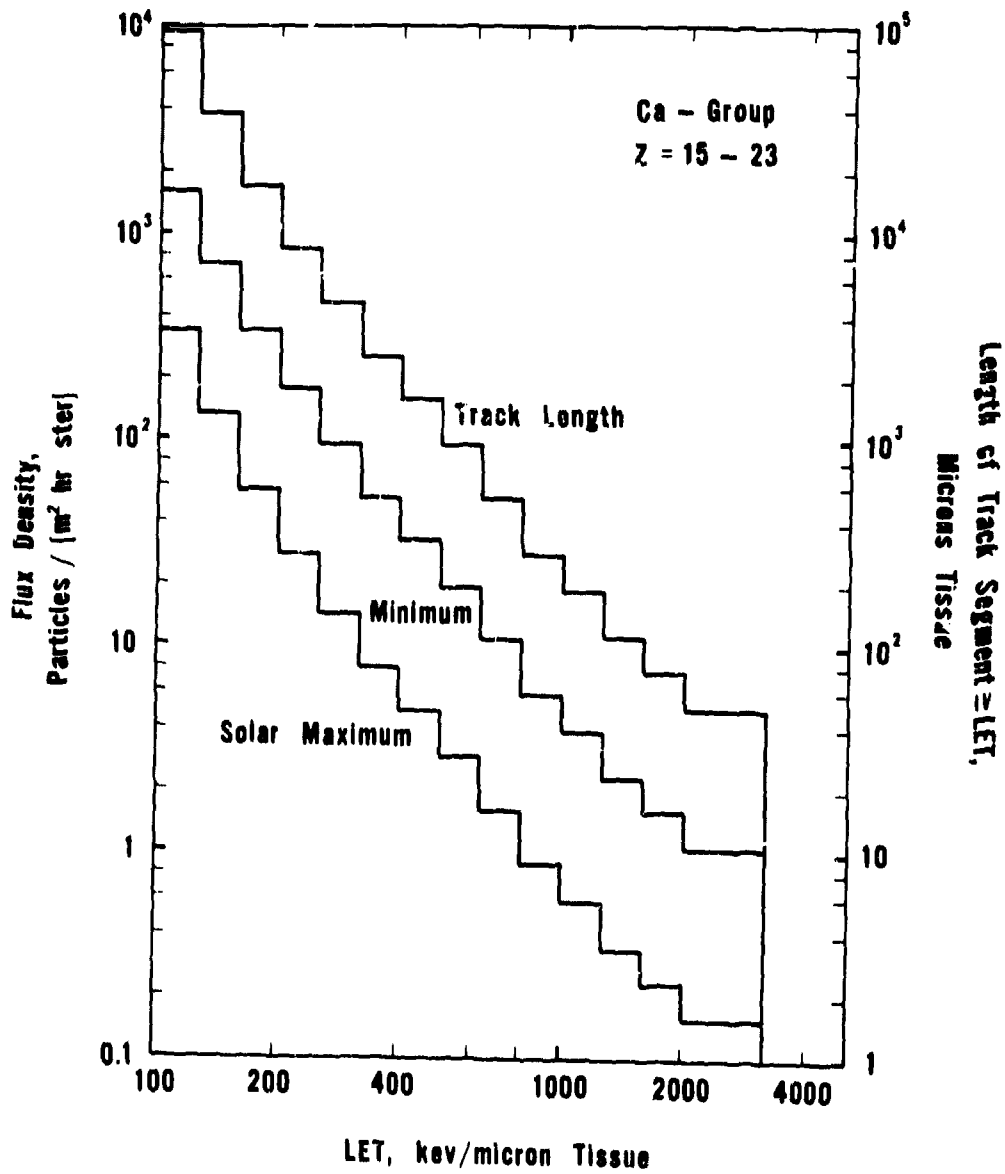**OF DIFFERENT Z NUMBERS**

FIGURE 7

17

LET DISTRIBUTION OF FLUX DENSITY AND TRACK LENGTH
FOR MG — GROUP AT SOLAR MINIMUM AND MAXIMUM

FIGURE 8

LET Increments:

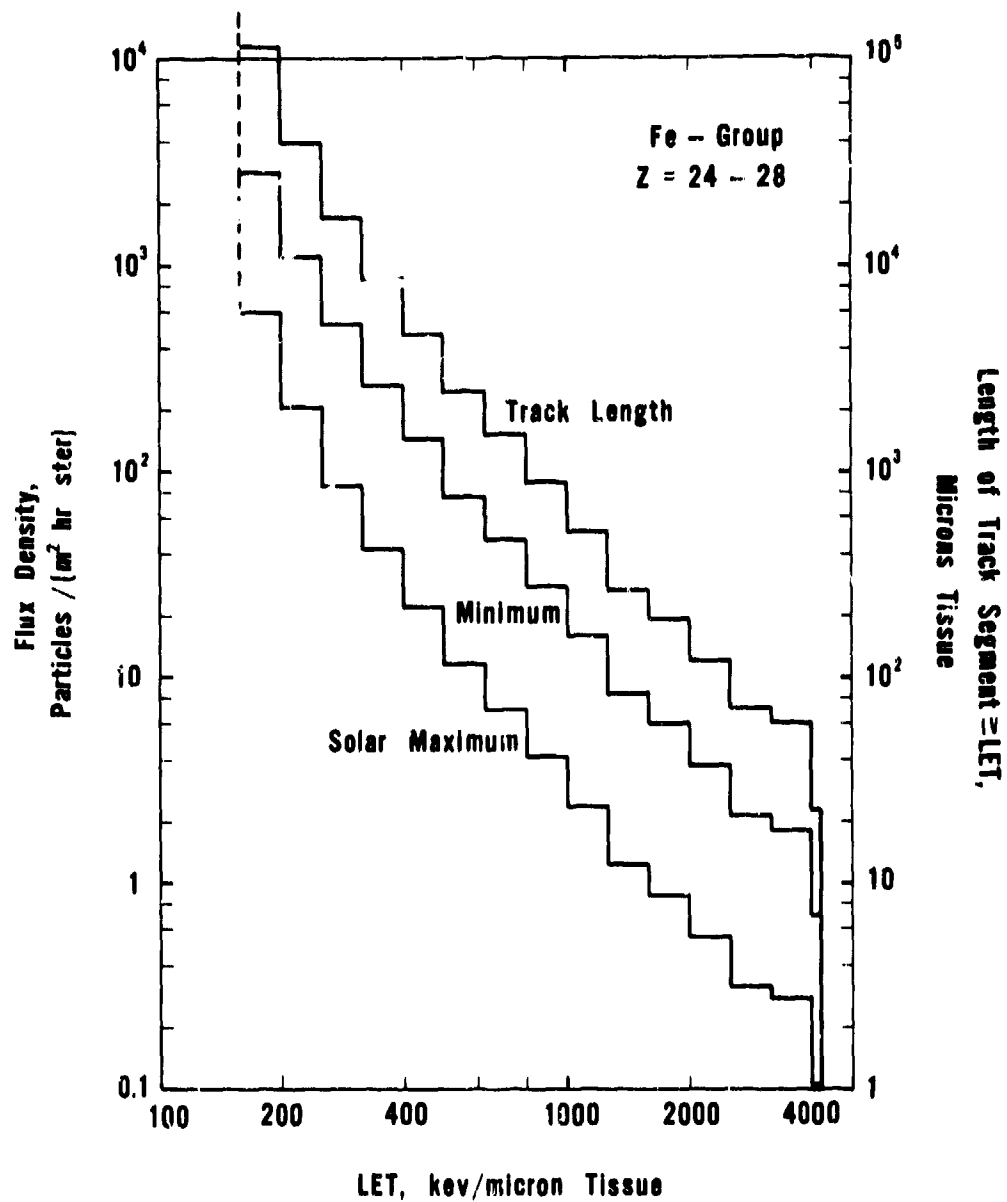| log LET:	2.0	2.1	2.2	2.3	2.4	2.5	2.6	2.7	2.8	2.9	3.0	3.2	3.238
LET:	100	126	159	200	251	316	398	501	631	794	1000	1590	1730

LET DISTRIBUTION OF FLUX DENSITY AND TRACK LENGTH
FOR CA – GROUP AT SOLAR MINIMUM AND MAXIMUM

FIGURE 9

LET Increments:

log LET:	2.0	2.1	2.2	2.3	2.4	2.5	2.6	2.7	2.8	2.9
LET:	100	126	159	200	251	316	398	501	631	794

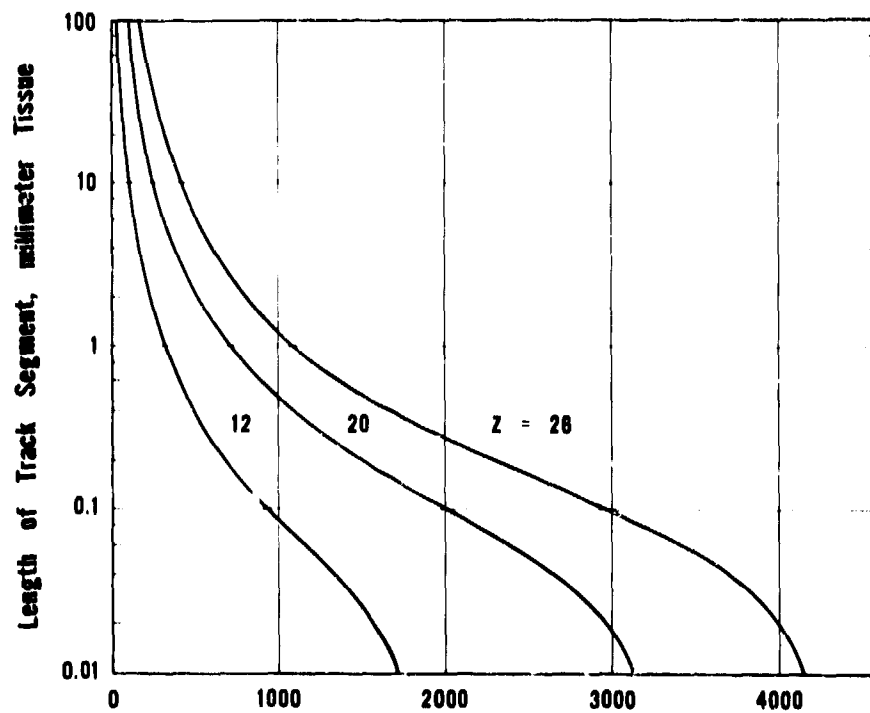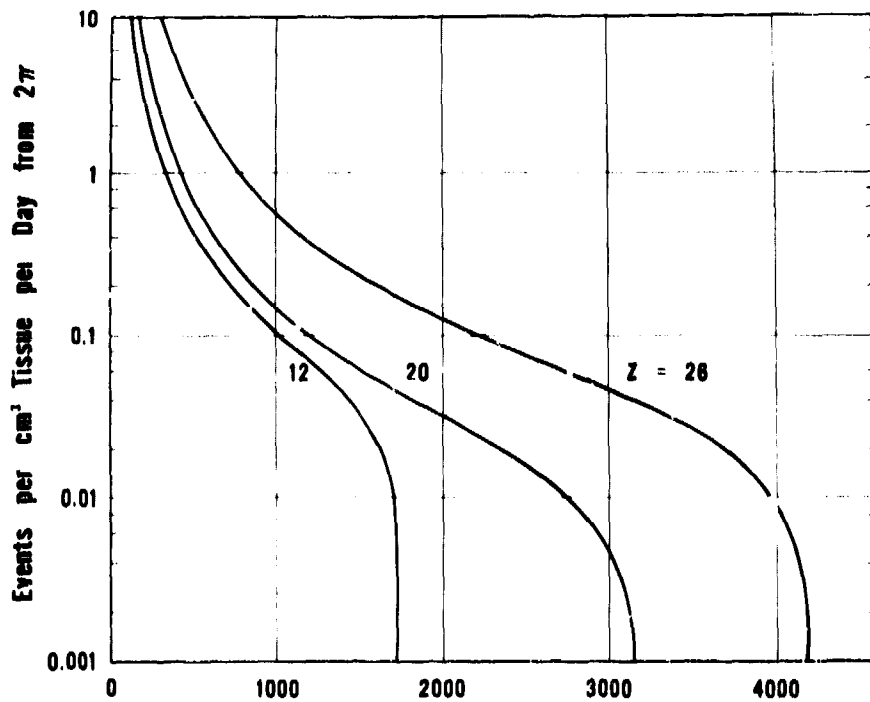| log LET:	3.0	3.1	3.2	3.3	3.5
LET:	1000	1260	1590	2000	3160

LET DISTRIBUTION OF FLUX DENSITY AND TRACK LENGTH FOR FE – GROUP AT SOLAR MINIMUM AND MAXIMUM

FIGURE 10

LET Increments:

log LET:	2.3	2.4	2.5	2.6	2.7	2.8	2.9	
LET:	200	251	316	398	501	639	794	

log LET:	3.0	3.1	3.2	3.3	3.4	3.5	3.6	3.62
LET:	1000	1260	1590	2000	2510	3160	3980	4180

20

SIZE AND FREQUENCY OF HZE PARTICLE
EVENTS IN TISSUE AT SOLAR MINIMUM

FIGURE 11